REVIEW

Corrected: Author Correction

https://doi.org/10.1038/s41586-018-0252-6

El Niño–Southern Oscillation complexity

Axel Timmermann[1,2,3]*, Soon-Il An[4], Jong-Seong Kug[5], Fei-Fei Jin[6], Wenju Cai[7,8,9], Antonietta Capotondi[10,11], Kim M. Cobb[12], Matthieu Lengaigne[13], Michael J. McPhaden[14], Malte F. Stuecker[15,16], Karl Stein[1,2], Andrew T. Wittenberg[17], Kyung-Sook Yun[1,2], Tobias Bayr[18], Han-Ching Chen[19], Yoshimitsu Chikamoto[20], Boris Dewitte[21,22], Dietmar Dommenget[23], Pamela Grothe[24], Eric Guilyardi[25,26], Yoo-Geun Ham[27], Michiya Hayashi[6], Sarah Ineson[28], Daehyun Kang[29], Sunyong Kim[5], WonMoo Kim[30], June-Yi Lee[1,2], Tim Li[3,6], Jing-Jia Luo[31], Shayne McGregor[23], Yann Planton[25], Scott Power[31], Harun Rashid[7], Hong-Li Ren[32], Agus Santoso[33], Ken Takahashi[34], Alexander Todd[35], Guomin Wang[31], Guojian Wang[7], Ruihuang Xie[36], Woo-Hyun Yang[5], Sang-Wook Yeh[37], Jinho Yoon[38], Elke Zeller[1,2] & Xuebin Zhang[39]

El Niño events are characterized by surface warming of the tropical Pacific Ocean and weakening of equatorial trade winds that occur every few years. Such conditions are accompanied by changes in atmospheric and oceanic circulation, affecting global climate, marine and terrestrial ecosystems, fisheries and human activities. The alternation of warm El Niño and cold La Niña conditions, referred to as the El Niño–Southern Oscillation (ENSO), represents the strongest year-to-year fluctuation of the global climate system. Here we provide a synopsis of our current understanding of the spatio-temporal complexity of this important climate mode and its influence on the Earth system.

The view on the El Niño phenomenon—originally described in 1893 as 'corriente del Niño'[1], a warm regional ocean current that affected climate off the coast of Peru—has changed over the past century. In the 1960s, ENSO was recognized as a basin-scale phenomenon involving coupled atmosphere–ocean processes[2]. A major international research programme in the 1980s and 1990s fundamentally advanced the ability to observe, understand and predict ENSO and its world-wide impacts[3]. During the past 20 years, our understanding of ENSO has continued to evolve, as new layers of complexity (Box 1) have been identified in ENSO dynamics and predictability. The concept of El Niño has developed from one of a canonical progression of phases from onset to maturity and demise[4] (Fig. 1) to one that accounts for its spatio-temporal complexity (Fig. 2) and varying climatic impacts[5–8] (Fig. 3). We have also come to realize that although ENSO primarily manifests itself as a year-to-year climate fluctuation, its dynamics involves a broad range of processes interacting on timescales that range from weeks[9,10] to decades[11]. Here the diversity in patterns, amplitude and temporal evolution of this climate phenomenon will be referred to as ENSO complexity (Box 1).

The most recent El Niño event[12], in 2015/2016, was initiated in boreal spring by a series of westerly wind events (WWEs) (Box 1, Fig. 3e)—a form of tropical weather noise. The associated wind forcing triggered downwelling oceanic Kelvin waves (Box 1, Fig. 1c), thus reducing the upwelling of cold subsurface waters in the eastern Pacific cold tongue (Box 1) and leading to surface warming in the central and eastern Pacific. The positive sea surface temperature anomaly (SSTA) shifted atmospheric convection from the Western Pacific Warm Pool (Box 1) to the central equatorial Pacific, causing a reduction in equatorial trade winds, which in turn intensified surface warming through the positive Bjerknes feedback (Box 1). The seasonally paced termination of the 2015/2016 event (Fig. 3e) was associated with ocean dynamics and the slow discharge of equatorial heat into off-equatorial regions, thus providing a delayed negative feedback (Box 1). The event started to decline in early 2016 and transitioned into a weak La Niña in mid-2016.

In broad terms, this evolution is common to the other strong El Niño events (Fig. 1), in 1982/1983 and 1997/1998 (Fig. 3c). However, no two events are alike—be they strong, moderate or weak (Figs. 2, 3f–m). This diversity arises from the varying roles of noise forcing (Fig. 3c–e) and of positive and negative coupled atmosphere–ocean feedback processes[13] (Box 1) that act to enhance and suppress the growth of SSTAs, respectively. The complexity of ENSO (Box 1), along with internal atmospheric noise, also translates into a diversity of global impacts[7,14]. When the underlying sea surface temperatures (SSTs) change in the equatorial Pacific, there are shifts in atmospheric deep convection, which in turn cause adjustments of the global Walker circulation (Box 1) and generate stationary atmospheric waves[15] that impact the far reaches of our planet. This perturbed global circulation influences weather variability, leading

[1]Center for Climate Physics, Institute for Basic Science (IBS), Busan, South Korea. [2]Pusan National University, Busan, South Korea. [3]International Pacific Research Center, University of Hawaii at Manoa, Honolulu, HI, USA. [4]Department of Atmospheric Sciences, Yonsei University, Seoul, South Korea. [5]Division of Environmental Science and Engineering, Pohang University of Science and Technology (POSTECH), Pohang, South Korea. [6]Department of Atmospheric Science, SOEST, University of Hawaii at Manoa, Honolulu, HI, USA. [7]CSIRO Oceans and Atmosphere, Aspendale, Victoria, Australia. [8]Physical Oceanography Laboratory/CIMST, Ocean University of China and Qingdao National Laboratory for Marine Science and Technology, Qingdao, China. [9]Centre for Southern Hemisphere Oceans Research (CSHOR), CSIRO Oceans and Atmosphere, Hobart, Tasmania, Australia. [10]Cooperative Institute for Research in Environmental Science, University of Colorado, Boulder, CO, USA. [11]Physical Sciences Division, NOAA Earth System Research Laboratory, Boulder, CO, USA. [12]Earth and Atmospheric Sciences, Georgia Tech, Atlanta, GA, USA. [13]LOCEAN/IPSL, Sorbonne Universités/UPMC-CNRS-IRD-MNHN, Paris, France. [14]Pacific Marine Environmental Laboratory/NOAA, Seattle, WA, USA. [15]Department of Atmospheric Sciences, University of Washington, Seattle, WA, USA. [16]Cooperative Programs for the Advancement of Earth System Science, University Corporation for Atmospheric Research, Boulder, CO, USA. [17]Geophysical Fluid Dynamics Laboratory/NOAA, Princeton, NJ, USA. [18]GEOMAR Helmholtz Centre for Ocean Research, Kiel, Germany. [19]Department of Atmospheric Sciences, National Taiwan University, Taipei, Taiwan. [20]Department of Plants, Soils, and Climate, Utah State University, Logan, UT, USA. [21]Centro de Estudios Avanzado en Zonas Áridas (CEAZA), Coquimbo, Chile. [22]Laboratoire d'Etudes en Géophysique et Océanographie Spatiale, Toulouse, France. [23]School of Earth, Atmosphere and Environment, Monash University, Clayton, Victoria, Australia. [24]Department of Earth and Environmental Sciences, University of Mary Washington, Fredericksburg, VA, USA. [25]Laboratoire d'Océanographie et du Climat: Expérimentation et Approches Numériques (LOCEAN), IRD/UPMC/CNRS/MNHN, Paris, France. [26]NCAS-Climate, University of Reading, Reading, UK. [27]Department of Oceanography, Chonnam National University, Gwangju, South Korea. [28]Met Office Hadley Centre, Exeter, UK. [29]School of Urban and Environmental Engineering, Ulsan National Institute of Science and Technology, Ulsan, South Korea. [30]Climate Prediction Department, APEC Climate Center, Busan, South Korea. [31]Australian Bureau of Meteorology, Melbourne, Victoria, Australia. [32]Laboratory for Climate Studies, National Climate Center, China Meteorological Administration, Beijing, China. [33]ARC Centre of Excellence for Climate System Science, Faculty of Science, University of New South Wales, Sydney, New South Wales, Australia. [34]Instituto Geofisico del Peru, Lima, Peru. [35]University of Exeter College of Engineering, Mathematics and Physical Sciences, Exeter, UK. [36]Institute of Oceanology, Chinese Academy of Sciences, Qingdao, China. [37]Department of Marine Sciences and Convergent Technology, Hanyang University, Ansan, South Korea. [38]School of Earth Sciences and Environmental Engineering, Gwangju Institute of Science and Technology, Gwangju, South Korea. [39]CSIRO Ocean and Atmosphere, Hobart, Tasmania, Australia. *e-mail: timmermann@pusan.ac.kr

Box 1

ENSO glossary

Bjerknes feedback. Positive ENSO feedback along the Equator, in which a weakened (strengthened) equatorial zonal sea surface temperature (SST) gradient weakens (strengthens) trade winds, which in turn further reduce (increase) the zonal SST gradient.

Combination tones/C-mode. Enhanced spectral energy on timescales of 9 months and 15–18 months, generated by the nonlinear modulation of ENSO by the seasonal cycle, and vice versa. C-modes play an important part in the seasonal turnabout of El Niño events.

Eastern Pacific cold tongue. An eastern equatorial Pacific region characterized by wind-driven upwelling of cold subsurface waters (Fig. 1a, b). The cold tongue warms considerably during eastern Pacific El Niño events and cools during La Niña events.

Ekman feedback. Positive (negative) SST anomalies (SSTAs) weaken (strengthen) the equatorial trade winds, reducing (increasing) the upwelling of cold subsurface water in the eastern equatorial Pacific, thus reinforcing the original SSTA.

ENSO complexity. ENSO complexity expands on the concept of ENSO 'pattern diversity' to include also temporal characteristics (from weather, annual cycle, interannual to decadal timescales), dynamics, predictability and global impacts.

ENSO skewness. Amplitude asymmetry of El Niño and La Niña events, which quantifies the fact that El Niño events attain larger amplitudes than La Niña events. Skewness is a clear indication of nonlinearity in the ENSO cycle.

Equatorial Kelvin wave: Eastward-propagating oceanic internal wave that displaces the interface (thermocline) between warm surface waters and cold subsurface waters. Westerly (easterly) equatorial wind anomalies generate downwelling (upwelling) Kelvin waves, which deepen (shoal) the thermocline in the eastern Pacific and reduce (enhance) the efficiency of climatological upwelling.

Multiplicative noise. Interaction between westerly wind events and underlying SST in the western and central Pacific, in which warmer (colder) SST favours more (fewer) westerly wind events; also referred to as state-dependent noise.

Recharge/discharge. Meridional transport of heat into/out of an equatorial band, driven by changes in near-equatorial wind variations. Recharge/discharge processes have a key role in the initiation and termination of El Niño events.

Thermal damping. Typically a negative feedback arising from SST-induced changes in surface radiative and turbulent heat fluxes in the tropical Pacific. It involves tropical clouds, convection and atmospheric boundary layer physics.

Thermocline feedback. Generally positive feedback operating in the eastern equatorial Pacific, in which a warm (cold) equatorial SSTA weakens (strengthens) equatorial trade winds, leading to mean upwelling of anomalously warm (cold) water.

Westerly wind event: Weather systems in the western and central Pacific that are often associated with an abrupt relaxation of the equatorial trade winds, generating downwelling Kelvin waves and an eastward expansion of the Western Pacific Warm Pool.

Western Pacific Warm Pool. Some of the warmest waters in the worlds' oceans occur in the western tropical Pacific, with temperatures exceeding 28 °C (Fig. 1a, b). The Western Pacific Warm Pool's seasonal north–south migrations have an important role in the termination of El Niño events.

Zonal advective feedback: Positive feedback, particularly effective in the central Pacific, in which a positive (negative) equatorial SSTA weakens (strengthens) equatorial trade winds, reducing (enhancing) the oceanic transport of cold waters from the eastern Pacific.

to massive reorganizations of tropical and extratropical temperature and rainfall patterns[16,17] (Fig. 3f–m).

Palaeo-climate reconstructions of the ENSO phenomenon covering the past ~10,000 years also show a wide range of amplitudes[18], thus highlighting the importance of internal climate processes in modulating ENSO complexity on timescales ranging from decades to centuries. In addition, the activity of reconstructed ENSO variability shows an intensification in the late 20th century relative to other pre-industrial periods[18,19], thus raising the general question of whether external forcings could influence the evolution and amplitude of ENSO. How ENSO responds to greenhouse warming is one of the most compelling outstanding questions[20].

Given the societal and environmental relevance of ENSO, it is paramount to improve our understanding of the processes that control the amplitude, timing, duration, predictability and global impacts of ENSO. Here we assess our current understanding of ENSO dynamical processes and their role in controlling complexity of this fundamental climate feature. Against this backdrop, we highlight areas of uncertainty (see 'A unifying framework') as a stimulus for further research.

A conceptual view of ENSO dynamics

Early efforts to elucidate the dynamics of ENSO focused on the average (composite) evolution of El Niño events[21], capturing the typical evolution of ocean and atmosphere conditions from the early-spring initiation of El Niño, to its winter-time peak and transition to La Niña during the subsequent summer (Fig. 1). The enhanced spectral interannual variability of ENSO (Fig. 3a, b) has been explained by invoking positive atmosphere and ocean feedbacks and delayed negative ocean adjustment feedbacks (Box 1), which together can lead to oscillatory dynamics, as encapsulated by a variety of conceptual ENSO models[22]. Here we focus on the ENSO recharge oscillator model[23] which, in its most general form, can be expressed as:

$$\begin{aligned} \mathrm{d}T_\mathrm{e}/\mathrm{d}t &= I_\mathrm{BJ}T_\mathrm{e} + Fh \\ \mathrm{d}h/\mathrm{d}t &= -\varepsilon h - \alpha T_\mathrm{e} \end{aligned} \quad (1)$$

where T_e and h represent the equatorial eastern Pacific surface temperature and zonal mean thermocline depth, respectively, and $\mathrm{d}T_\mathrm{e}/\mathrm{d}t$ and $\mathrm{d}h/\mathrm{d}t$ are the corresponding time derivatives. The Bjerknes stability index, I_BJ, (also referred to as the BJ index or ENSO linear growth rate; Fig. 1j) depends on a number of processes (such as thermocline, zonal advective and Ekman feedbacks) that reinforce SST, and on negative feedbacks from thermal advection by horizontal mean surface currents and thermal damping by net surface heat fluxes[13] (Box 1). In equation (1), ε represents the damping rate of thermocline depth anomalies. The interannual timescale of the ENSO system is mainly determined by F and α, which describe the thermocline feedback (Box 1) and the slow equatorial recharge–discharge process (Box 1) associated with oceanic heat transport, respectively. For a constant I_BJ, the model describes a linear recharge oscillator: starting from neutral conditions with $T_\mathrm{e} \approx 0$ (typically in boreal winter–spring; Figs. 1c, 2) and a charged thermocline state, $h > 0$, an El Niño event can grow (Figs. 1d, e, 2). While eastern equatorial Pacific SSTAs develop, the thermocline feedback, Fh, (Box 1) further intensifies the growth of the SSTAs by upwelling anomalously warm subsurface waters to the surface in the eastern Pacific cold tongue. Moreover, positive eastern Pacific SSTAs $(T_\mathrm{e} > 0)$ cause a weakening of the equatorial trade winds (Fig. 1d, e). The associated wind-stress curl discharges the equatorial heat through Sverdrup transport (Box 1) and ocean boundary processes (Fig. 1f). The resulting drainage of heat in turn weakens the thermocline feedback, and the phase of the ENSO recharge oscillator can transition into a La Niña state (Fig. 1g, h), which is accompanied by recharging of heat through opposite wind-stress curl anomalies (Fig. 1h).

Comparing the linear oscillator solution of equation (1) (constant I_BJ) with the scatter plot of observed equatorial eastern Pacific temperature and zonal mean thermocline depth anomalies (Fig. 2),

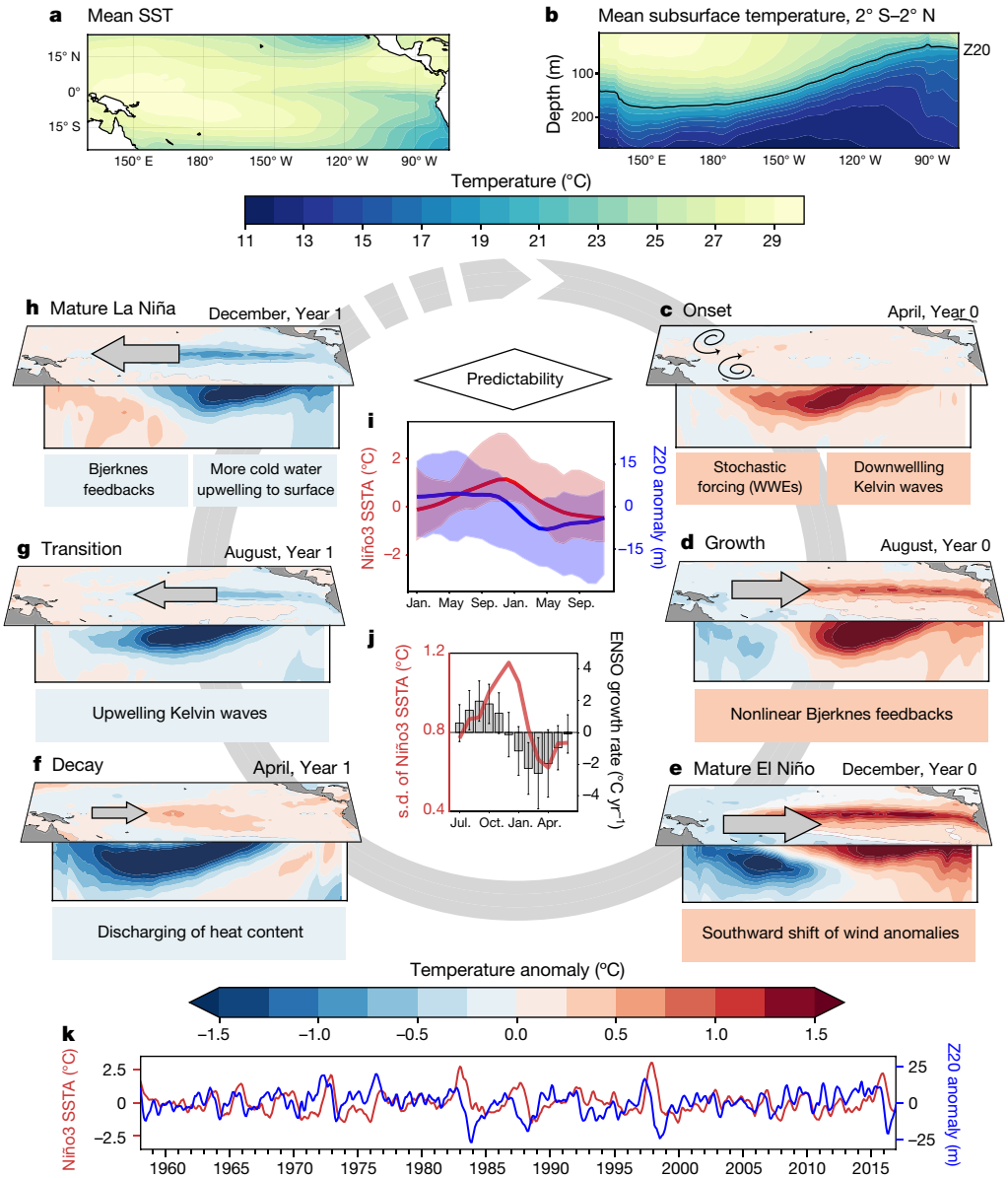

Fig. 1 | ENSO cycle. Composite evolution of El Niño events from 1958 to 2015. **a**, **b**, Mean SST[26] (**a**) and subsurface potential temperature[96] (**b**) between 2° N and 2° S. The depth of the 20 °C isotherm (Z20) is indicated by the black line. **c**–**h**, Composite SSTAs[26] and subsurface temperature anomalies[96] from 17 El Niño events (1963, 1965, 1968, 1969, 1972, 1976, 1977, 1982, 1986, 1987, 1991, 1994, 1997, 2002, 2004, 2006 and 2009), based on the 0.5 °C exceedance of the three-month running mean of the NOAA ERSST.v5 (Extended Reconstructed Sea Surface Temperature dataset, version 5) SSTAs[97] in the Niño3.4 region (averaged over 5° S–5° N and 120° W–170° W). The arrows represent wind anomalies and the boxes list major processes involved in the phases of El Niño evolution. **i**, The seasonal composite means (lines) and spread (shading) of eastern equatorial Pacific SSTA (red; averaged over the Niño3 region: 5° S–5° N and 90° W–150° W) and equatorial Pacific zonal mean Z20 (blue) for the 17 El Niño events. The diamond illustrates that ENSO predictability increases with increasing ENSO signal strength. **j**, The monthly standard deviation (s.d.) of the Niño3 SSTA[26] (red line) and an estimate of the monthly ENSO growth rate based on the Bjerknes stability index. The error bars show the 90% confidence range for the index calculated from the standard error of the regression slope[56]. **k**, Time series of the Niño3 SSTA and zonal mean equatorial Pacific depth anomaly from the 20 °C isotherm (2° S–2°N and 120° E–80° W) from the merged data product[27,98].

we find substantial differences. The observed scatter diagram shows a high degree of irregularity and a notable positive skewness in eastern tropical Pacific SSTAs towards El Niño events (Box 1, Fig. 2). El Niño and La Niña events are very different in terms of their amplitude and time evolution (Figs. 1k, 2a). To account for this additional level of complexity, the simple recharge oscillator model can be extended by including a nonlinear Bjerknes feedback term that represents either atmospheric or oceanic nonlinear processes[24] or multiplicative stochastic forcing[25] (Box 1). For these extensions, the recharge model can then simulate the skewed probability distribution of ENSO (Fig. 2) and the fast growth from neutral to strong El Niño conditions (Fig. 1j). The observed positive skewness of the SSTA (Fig. 2), which indicates the importance of nonlinear dynamical and thermodynamical processes in the coupled tropical Pacific climate system, implies that strong El Niño conditions, which typically last for one year, are on average shorter than La Niña events, which can persist for up to several years (Fig. 1k).

Whereas conceptual models like equation (1) can simulate some key features of ENSO evolution, they can neither explain the presence of its spatial diversity (Fig. 3a, b, f–m) nor the potential remote effects of variability originating from the extra-tropical Pacific, Atlantic or Indian Ocean onto this diversity. An improved framework to characterize and explain ENSO complexity is needed to capture these aspects.

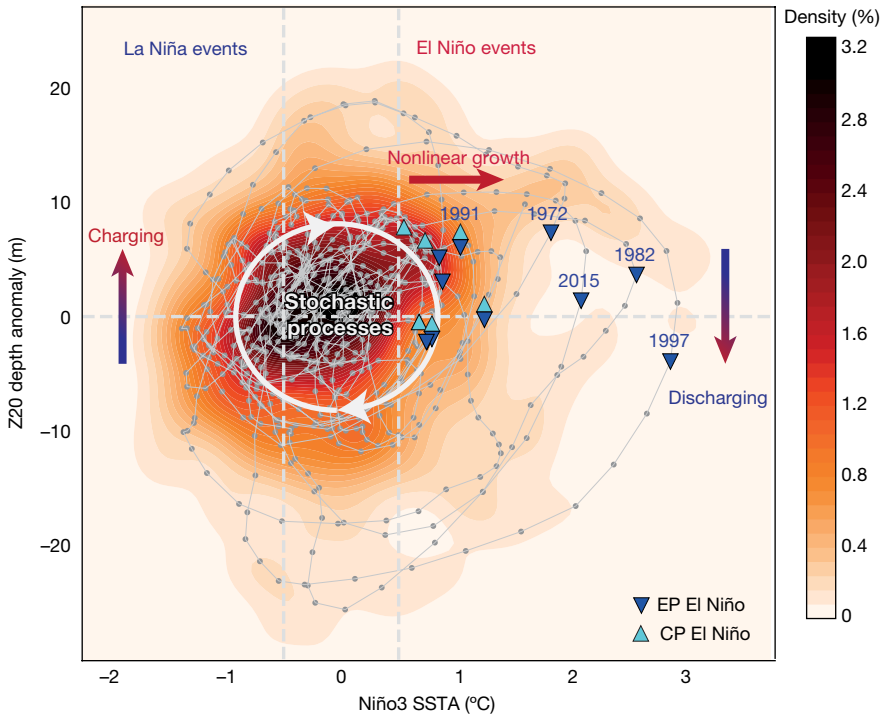

Fig. 2 | Schematic representation of ENSO temporal complexity. Kernel density estimate of the joint probability distribution (orange shading) of the linearly detrended Niño3 SSTA and zonal mean 20 °C isotherm depth anomalies (2° S–2° N and 120° E–80° W) for the period 1958–2016 from the merged data product[27,98]. The grey circles indicate the monthly values of the two time series, smoothed with a three-month running mean filter. Dark and light-blue triangles indicate December values of EP (1972, 1976, 1982, 1986, 1997, 2006 and 2015) and CP (1968, 1994 and 2009) El Niños, respectively. Mixed events (1965, 1991 and 2002) are represented by combined dark and light-blue triangles. The years of the five largest El Niño events are indicated. The white ellipse in the centre corresponds to the progression of the linear recharge oscillator, and arrows on the left (right) indicate charging (discharging) of subsurface warm water in the equatorial Pacific.

Space–time complexity of ENSO

Despite some prominent commonalities discussed in the previous section (Fig. 1), El Niño events differ considerably from each other in terms of magnitude, spatial pattern, temporal evolution and predictability[5–7] (Figs. 2, 3f–m). To characterize the leading modes of equatorial Pacific SST variability and their diverse timescales, we conduct an empirical orthogonal function (EOF) analysis of observed tropical Pacific SSTAs[26] (Fig. 3), which identifies the leading orthogonal patterns of variability. The leading EOF (Fig. 3a), which corresponds to the classical El Niño pattern with eastern tropical Pacific warming, exhibits variability on quasi-quadrennial timescales (3–7 years; spectral density estimate in Fig. 3a). By contrast, the second EOF, which explains only 25% of the variance of the first mode, is characterized by an east–west zonal SST dipole in the tropical Pacific and has enhanced variance on quasi-biennial and decadal timescales (spectral density estimate in Fig. 3b). The interplay of these two EOFs largely captures the spatial diversity of the observed ENSO mode.

Some El Niño events (for example, that of 1997/1998) are characterized by pronounced warming in the eastern Pacific and are referred to as EP El Niño events (Fig. 3c, f), whereas others (for example, that of 2004/2005) show a stronger positive projection on the second EOF mode, which leads to a more pronounced central Pacific warming, and are known as CP El Niño events (Fig. 3d, h–j). More generally, El Niño events can be viewed as the superposition of the two EOF modes, which results in a continuum of ENSO characteristics[27,28] that capture a mix of EP and CP dynamics (for example, the 1991/1992 and 2015/2016 events) (Fig. 2). La Niña events (for example, that of 1999/2000; Fig. 3g), in addition to being weaker than El Niño events, exhibit less diversity in their spatial patterns[6,29], thus clearly pointing to an asymmetry in the underlying dynamical processes for ENSO.

EP El Niño events (for example, that of 1997/1998; Fig. 3c) tend to involve basin-scale equatorial wind anomalies, a strong relaxation of the zonal tilt of the equatorial thermocline (Fig. 1e), a more prominent role for the thermocline feedback (Box 1), large eastward shifts of tropical Pacific convection and strong discharge of heat content (Fig. 3c) away from the equatorial region, which boosts the likelihood of transitioning into a La Niña event[6,30]. By contrast, CP El Niño events (for example, that of 2004/2005; Fig. 3d) tend to involve more local wind feedbacks, a stronger role for the zonal advective feedback (Box 1), little reduction in the zonal tilt of the thermocline, weak shifts of convection, earlier termination, little poleward discharge of ocean heat content (Fig. 3d), a stronger role for thermal damping (Box 1) during the decay phase, a reduced likelihood to transition into La Niña and more susceptibility to disruption by wind noise[6,30]. Compared to CP El Niños, strong EP El Niños also tend to terminate later in boreal spring owing to trade wind collapse, which suppresses the upwelling that normally connects the SST to the evolving thermocline depth[31].

The spatial diversity in the SSTA patterns of ENSO is also associated with different tropical precipitation patterns (Fig. 3f–m), resulting in potentially different remote teleconnection patterns and corresponding weather and climate impacts[7,32]. However, given the high level of internal atmospheric variability[33] and the brevity of the historical record, it has remained difficult to unequivocally detect the differences in the impacts of various ENSO spatial modes. In addition to its spatial diversity, ENSO also exhibits substantial diversity in its temporal evolution (Figs. 1k, 3c–e). Understanding this diversity of El Niño events is crucial for predicting the regional impacts of ENSO, for example, on precipitation patterns, tropical cyclones and other types of severe weather[5]. The extent to which El Niño diversity is predictable relates to whether ENSO complexity originates mainly from random processes or from low-frequency deterministic dynamics. Random processes affecting a single physical ENSO mode could generate diversity in amplitude, spatial structure and temporal evolution[8], consistent with a spatial flavour continuum generated by different realizations of atmospheric noise[27].

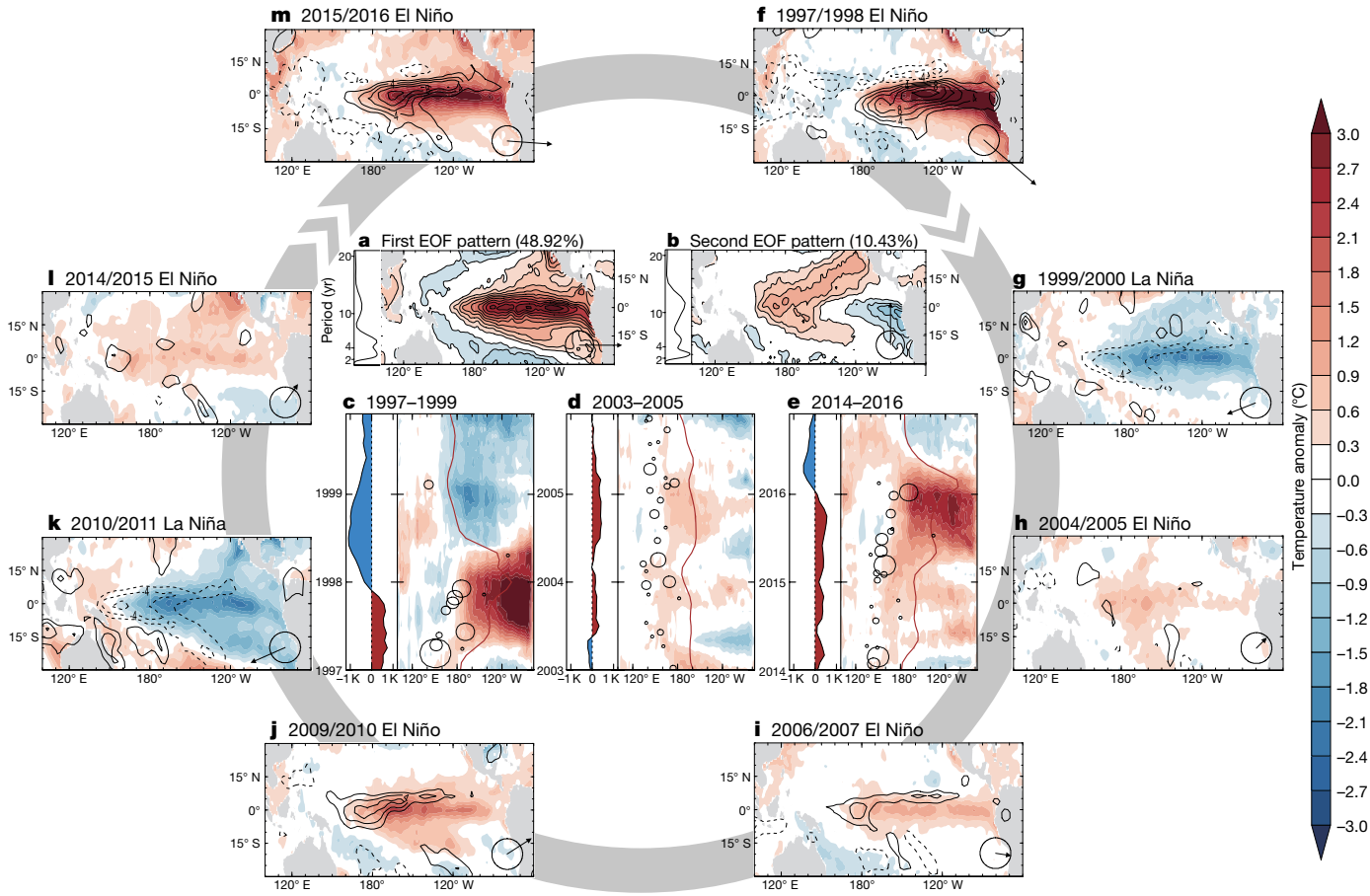

Fig. 3 | Spatio-temporal complexity of ENSO. a, **b**, First (**a**) and second (**b**) EOF patterns of a linearly detrended SSTA[95] computed for 25° S–25° N and 140° E–80° W during 1920–2016, with the associated variance-preserving spectral power density of the normalized principal components shown on the left (the vertical axis is the period in years and the horizontal axis is the logarithm of the power). Numbers in parentheses indicate the variance of the EOF modes. **c**–**e**, Longitude–time evolution of the Pacific SSTA averaged over 5° S–5° N for selected observed ENSO events, the 28.5 °C isotherm of the SST (red curve) representing the edge of the Western Pacific Warm Pool, the longitude and strength of WWEs[99] (black circles) and (on the left) the associated equatorial Pacific heat-content anomaly (temperature anomaly averaged over the top 300 m of the ocean and between 5° S–5° N and 120° E–90° W; range from −1 K to 1 K; red, positive; blue, negative). **f**–**m**, Spatial pattern of SSTA (shaded) and precipitation anomaly[100] (contours; solid line, positive; dashed line, negative; 2 mm d^{-1} interval; zero contour omitted) averaged over the November–January season of selected ENSO events. We note that strong warm events (1997/98 and 2015/16) induce very strong eastward and equatorward shifts of rainfall. At the bottom right of **a**, **b** and **f**–**m** we show the associated principal components (PCs); namely, the projection of each SSTA spatial pattern onto the EOF patterns in **a** and **b**. The abscissa is PC1, the ordinate is PC2 and the arrow length is proportional to the magnitude in PC1–PC2 space (an arrow magnitude of 1 is indicated by the circles).

Alternatively, initial subsurface ocean conditions could modulate the role of stochastic wind forcing in producing diversity. For example, climate model simulations have demonstrated that in the presence of stochastic WWEs, an initial build-up of equatorial Pacific upper-ocean heat content can favour the development of EP, rather than CP, El Niño events[10,34] (Fig. 3d, e). At the onset of strong El Niño events[35], such as those of 1997/1998 and 2015/2016 (Fig. 3c, e), WWE activity tends to strengthen and expand eastwards with the expansion of the Western Pacific Warm Pool and the relaxation of the trade winds. These WWE changes can be parameterized in equation (1) as multiplicative noise (Box 1), which can contribute to ENSO diversity and asymmetries[9,36].

Studies suggest that ENSO diversity may be triggered by climate phenomena outside the tropical Pacific, including the North[37] and South[38] Pacific meridional modes, extra-tropical atmospheric circulation patterns and tropical Atlantic variability[5,39,40]. For example, the negative phase of the North Pacific Oscillation[41] tends to favour the development of positive SSTAs in the central Pacific by weakening the trade winds in the Northern Hemisphere, while the positive phase of the South Pacific Oscillation tends to weaken the Southern Hemisphere trade winds, thereby favouring the development of positive SSTAs in the eastern Pacific. Such remote influences appear to be mediated primarily by how they project onto wind variations in the equatorial Pacific. In essence, westerly wind anomalies in the western equatorial Pacific tend to favour CP El Niños, whereas westerly wind anomalies in the central–eastern equatorial Pacific tend to favour EP El Niños. These external influences can precede the peak of El Niño by 2–3 seasons[39,41] and may provide additional predictability to the spatial characteristics of an emerging El Niño event.

Since 1998, CP events have become more prevalent than EP events[42]. Such a decadal modulation in ENSO diversity is consistent with coupled general circulation models (CGCMs) that can spontaneously generate multidecadal variations in ENSO diversity even in the absence of external radiative forcings[43]. Low-frequency climatic drivers (including natural and anthropogenic forcings)—which involve basin-wide changes in the zonal SST gradient, thermocline depth and winds[44,45]—may also have contributed to the observed decadal swings in ENSO diversity by favouring particular spatio-temporal modes[46]. At this stage, the observational record remains too short to quantify all the possible sources of the decadal modulation of ENSO characteristics.

The current generation of climate models underestimates ENSO diversity[47]. This issue is related to the models' systematic biases, which affect the mean state and ENSO feedbacks. Sources of these biases include deficiencies in the simulation of clouds, atmospheric convection and oceanic mixing[48]. In particular, atmospheric model responses

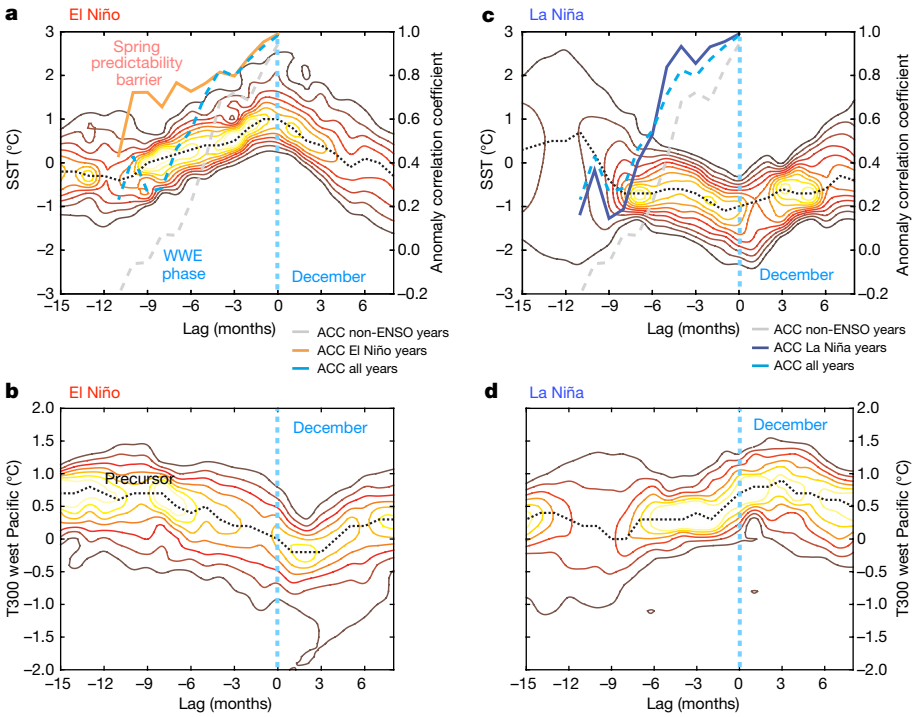

Fig. 4 | Probabilistic ENSO precursors and predictive skill. a, **c**, Time-evolving Kernel density probability density estimates (contours) of the linearly detrended eastern equatorial Pacific SSTA[26] (averaged over the Niño3.4 region: 5° S–5° N and 170° W–120° W) for the period 1958–2016 for El Niño (**a**) and La Niña (**c**) conditions, exceeding the +0.5 °C and −0.5 °C threshold, respectively. **b**, **d**, The same as **a** and **c**, but for western tropical Pacific heat-content anomalies[96]—namely, temperature anomalies averaged over 5° S–5° N, 120° E–155° W and 0–300 m (T300) and high-pass-filtered with a cut-off period of 20 years to remove multi-decadal trends. Every time the probability for SSTAs (heat-content anomalies) to be in the range from −3 °C to 3 °C (−2 °C to 2 °C) is ~100%. However, some SSTA and heat-content values are more likely to occur than others. This probability is indicated by the coloured contours (probability contour interval, 0.005). The time evolution of the probability density estimates is shown for different lead and lag times, relative to El Niño and La Niña events peaking in December. Black dotted lines correspond to the maximum probability for each lag. Thick lines in **a** represent the anomaly correlation coefficient skill (ACC) for the December Niño3.4 SSTA[97] (1980–2015) exceeding +0.5 °C (orange), within the range −0.5 °C to +0.5 °C (grey) and for all years (cyan), calculated using nine coupled models from the North American Multimodel Ensemble project[77]. Lines in **c** are the same as in **a**, but for anomalies below −0.5 °C (dark blue), within the range −0.5 °C to +0.5 °C (grey) and all years (cyan). We note that the ACC shown here in orange and dark blue lines does not represent the skill aggregated over all initial conditions, but only over those identified a posteriori as El Niño and La Niña events.

tend to be relatively insensitive to distinct patterns of SSTAs owing to climatological dry and cold biases in the equatorial central Pacific[47,49].

Seasonal ENSO dynamics

ENSO displays a close relationship with the seasonal cycle[21,50]: El Niño events usually start in boreal spring (Figs. 1c, i, 4), grow during the summer and autumn (Fig. 1d), reach their maximum intensity in winter (Fig. 1e, i) and decay rapidly during late winter and spring (Fig. 1f, j). In most cases, they transition to La Niña events (Figs. 1g, h, 4) by the subsequent summer. This seasonal synchronization of ENSO translates into the observed eastern equatorial Pacific SSTA variance peaking during boreal winter and attaining minimum values during spring (Fig. 1j). It also leads to pronounced seasonal contrasts in the climate impacts and predictability of ENSO (Fig. 1i). ENSO influences the global atmospheric circulation, affecting, for instance, the Asian monsoons[51] and the climate in America[52] and Australia[53].

Randomly occurring sequences of WWEs, typically during spring, can lead to an initial warming of the central eastern equatorial Pacific[54,55] (Fig. 1c). This initial SSTA can grow because the air–sea coupling is strongest in summer and early autumn[56,57] (Fig. 1j). Proposed physical processes for this summer–autumn coupling maximum include (i) the shift of the Intertropical Convergence Zone towards the Equator and its associated increase in western Pacific surface wind convergence[58], (ii) the seasonal outcropping of the equatorial thermocline[59], (iii) the seasonal cooling of the eastern equatorial Pacific[58] and (iv) the reduction of negative cloud feedbacks[60].

The decay of El Niño events typically starts in boreal winter. The anomalous westerly wind anomalies shift southwards from the Equator, leading to a shoaling of the eastern Pacific thermocline and a subsequent reduction of the overlying SSTA[61] (Figs. 1f, 4a). This shift arises from climatological expansion of the Western Pacific Warm Pool into the Southern Hemisphere, coincident with the development of the South Pacific Convergence Zone[62]. In this season, the increased surface heat flux damping[60] results in a decrease of the air–sea coupling strength (Fig. 1j), which—together with the aforementioned seasonal southward wind shift[63] and the equatorial heat content discharge[23] (Fig. 4b)—leads to a rapid transition to a La Niña state.

While these seasonal processes generally operate for different flavours and phases of ENSO, differences in their relative importance can contribute to ENSO complexity. For instance, CP events typically terminate earlier and are less likely to transition to a La Niña state compared to EP El Niño events[62] (Fig. 3d). Furthermore, La Niña conditions can last up to 2–3 years (Figs. 3c, 4b). The ability to simulate ENSO seasonal synchronization for different types of El Niño events varies strongly among the current generation of climate models, probably owing to biases in mean state and seasonal cycle[56].

The influence of the seasonal variations of the air–sea coupling strength discussed above can be included in the framework of the recharge oscillator (equation (1)) by adding a seasonally varying growth rate (I_{BJ}). As expected, this model then captures the observed ENSO seasonal synchronization characteristics, including the seasonal ENSO variance modulation and partial phase synchronization[25]. Interactions between the seasonal cycle in I_{BJ} and the interannual ENSO temperature signal generate variance with periods of roughly 9 and 15–18 months, the so-called combination tone frequencies (Box 1) that broaden the ENSO spectrum predominantly towards higher frequencies[64,65].

These interacting dynamics create specific atmospheric circulation patterns that are together referred to as combination mode[64] (C-mode) (Box 1). The spatial pattern of the C-mode exhibits a pronounced hemispheric asymmetry, which includes an anomalous cyclonic low-level wind circulation in the southern central tropical Pacific and an anomalous anticyclonic low-level wind circulation in the northwestern tropical Pacific. Some of the prominent local expressions are the aforementioned southward shift of equatorial wind anomalies[63] (Fig. 1e) and the anomalous western North Pacific anticyclone[65].

ENSO predictability

To link our understanding of dynamical tropical air–sea interactions with ENSO predictability, it is helpful to elucidate the seasonal evolution of (i) potential precursors that may contribute to long-term predictability[66] (9–15 months lead time), (ii) triggers that can rapidly increase the likelihood for event development (6–9 months lead time) and (iii) transition processes (see 'A conceptual view of ENSO dynamics' and 'Seasonal ENSO dynamics'). The development of a typical EP event can be divided into different seasonal stages, which each contribute differently to the boreal winter 6–9 month SSTA forecasting skill in the Niño 3.4 region (central to eastern Pacific), as illustrated by the anomaly correlation coefficient skill between seasonal forecasts performed with the North American Multimodel Ensemble[67] (NMME) and the observations (Fig. 4a, cyan dashed line). Prior to boreal spring, a charged western tropical Pacific heat content is a necessary condition for the subsequent development of El Niño events (Fig. 4b). Thus, the corresponding warm pool heat advection processes[68,69] have a key role in determining the long-term memory for ENSO forecasts. Furthermore, atmospheric precursors in the North[37] and South Pacific[38], the Indian Ocean[70] or the tropical Atlantic[40,71] have been suggested to influence the El Niño evolution for long lead times.

It must be emphasized here that the presence of such early oceanic or atmospheric precursors is usually not sufficient for El Niño growth because one of the key trigger mechanisms is the stochastic WWE activity in boreal spring and early summer[72]. This is clearly illustrated by the fact that even though initial heat-content conditions were favourable for El Niño development in early 2012, 2014 and 2017, the subsequent SSTA growth stayed below expectations. Individual WWEs are not predictable beyond the weather prediction horizon, which implies that, on average, forecasts initialized in boreal spring have relatively low long-term skill[73], in particular in the absence of precursor signals (Fig. 4a, cyan line). However, precursor signals in western tropical Pacific heat content (Fig. 4b) could be indicative of potentially developing El Niño conditions, which in effect enhance the predictability (Fig. 4a, orange line) relative to the averaged case (Fig. 4a, cyan line). The competing roles of stochasticity versus ocean memory for this so-called spring predictability barrier (Fig. 4a) and for long-lead-time forecasts have been intensely debated[74,75].

If a sufficient amount of westerly momentum is transferred in boreal spring from the atmosphere to the ocean, zonal advective processes begin moving the warm pool front eastwards, and downwelling Kelvin waves (Box 1) generate surface warming in the eastern tropical Pacific about two months later. These anomalies are further intensified (Fig. 4a) owing to increasing summer air–sea coupling strength (Fig. 1j), while anomalously warm water is drained from the Western Pacific Warm Pool (Fig. 4b). This phase exhibits a high degree of climate predictability, as documented by the high anomaly correlation coefficients (>0.6) between predicted boreal winter El Niño events and observations for forecasts initialized in boreal summer (Fig. 4a). The subsequent demise of an El Niño event is largely controlled by ocean subsurface processes and the discharge of zonal heat content away from the Equator (Figs. 1i, 2, equation (1)), as well as by the seasonally modulated southward shift of westerly wind anomalies[63], which in turn leads to a relaxation of the zonally integrated thermocline anomalies. This seasonally locked decay of El Niño conditions under a low-noise atmospheric environment further contributes to the long-term averaged ENSO prediction skill[62].

The subsequent evolution into a La Niña state (Fig. 4a–c) and the possibility of having multi-year La Niña events (Figs. 1k, 4c) are less well understood. La Niña events are often preceded by a strong El Niño. However, as indicated by the broad probability distribution of the SSTA at a lag of 9–15 months (Fig. 4c), other initial conditions can also develop into La Niña events peaking in boreal winter (Fig. 4c). During the transition from El Niño to La Niña, equatorial heat gets quickly discharged, and 6–9 months before a peak La Niña in boreal winter, we observe the smallest values of the equatorial heat content (Fig. 1i) and a slow recharging tendency of the Western Pacific Warm Pool (Fig. 4d). However, during this period the probability density of western tropical Pacific heat-content anomalies is relatively broad, which translates into an overall reduction of predictive skill (Fig. 4c). Because longer-lasting La Niña events are exposed to a variety of atmospheric and oceanic perturbations and the annual cycle, a dynamical decoupling of La Niña and subsequent El Niño events may occur[76]. In boreal winter, during the peak of the La Niña, the Western Pacific Warm Pool is fully charged (Fig. 4d) to values that are typical for an El Niño precursor (Fig. 4b). However, the SST conditions do not necessarily have to swing back to an El Niño state and sometimes even a second La Niña can develop. When comparing the anomaly correlation coefficient skill for December La Niña target conditions with the averaged skill for all years (1980–2015) from the NMME[77], we find very little difference (Fig. 4c) for lead times of 1–12 months, which suggests that (i) La Niña conditions have a considerably lower predictability than El Niño, (ii) the predictability of La Niña is to a first order captured well by the mean statistical skill of the current generation of seasonal prediction models. Using ensemble forecasting techniques, a recent study[78] identified potential predictors for the likelihood of multi-year La Niña events, which include the magnitude of thermocline discharge and the amplitude of the preceding El Niño event, suggesting the possibility for longer-term forecasts also for La Niña.

How the different stages of predictability differ between CP and EP events and whether there are distinct precursor patterns for different ENSO flavours still remains controversial[68,79]. Despite an improved understanding of ENSO dynamics, the ENSO prediction skill has not demonstrated a steady improvement during the past few decades, with even a decrease at the turn of the 21st century[73]. This decrease may be related to the reduced ENSO amplitude and the more frequent occurrence of CP events during that period[79], as their evolution and climate impacts tend to be less predictable than those of EP El Niño events[80].

A unifying framework

The previous discussion has highlighted a variety of dynamical pathways that can be combined to explain the spatio-temporal complexity of the ENSO phenomenon (Fig. 5). Extending beyond the simple single-mode theory (equation (1); 'A conceptual view of ENSO dynamics'), which captures several—but not all—features of ENSO dynamics, our proposed framework for ENSO complexity is based on the co-existence of a duplet of linear eigenmodes (Fig. 5a, b), which can be derived from a deterministic, intermediate-complexity tropical atmosphere and ocean model[46] and a number of excitation mechanisms. These two generic coupled eigenmodes are characterized by spatial patterns that closely resemble the observed EP and CP modes (Fig. 5) and by timescales of approximately four and two years, respectively. The four-year (quasi-quadrennial) mode is more prominent (Fig. 5, lower left) when the mean thermocline is deep and the trade winds are weak, and it relies strongly on thermocline feedback. By contrast, the two-year (quasi-biennial) mode is dominant when the mean thermocline is shallow and the equatorial trade winds are strong. Its SST variability is strongly controlled by zonal advective feedback[46]. These features are akin to their observational counterparts (Figs. 3, 5c, d). For realistic background states, both modes operate not far from criticality (zero growth rate) (Fig. 5, lower left), which implies that they can be easily excited by other processes. Their stability and excitability depends further on the prevailing climatic background conditions.

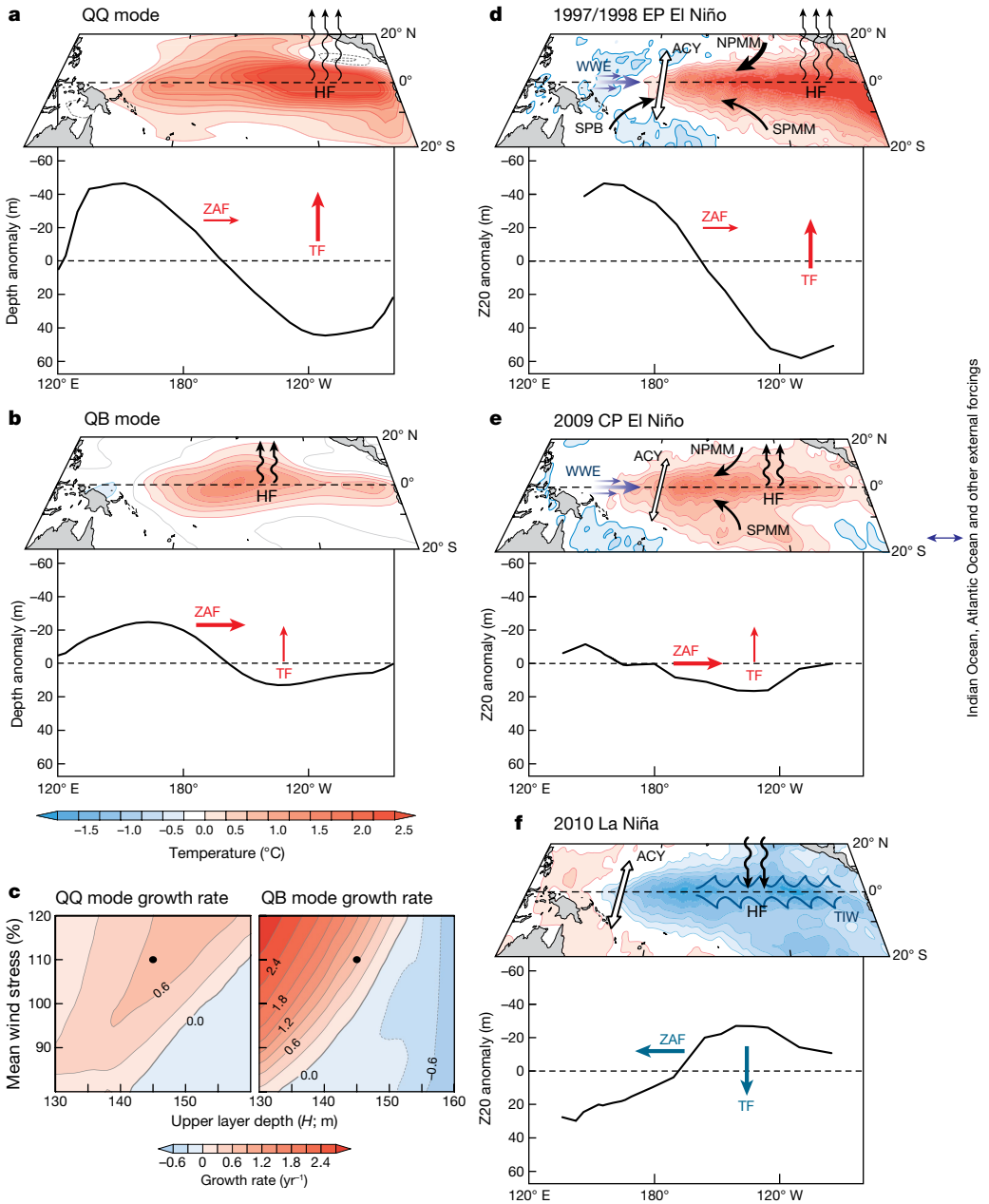

Fig. 5 | Mechanisms of ENSO complexity. a, **b**, Leading two eigenmodes of tropical Pacific SSTA and equatorial thermocline depth anomalies (averaged between 5° S–5° N) with periods of about 4 yr (QQ, quasi-quadrennial) and about 2 yr (QB, quasi-biennial), calculated fom an intermediate ENSO model[46]. The differences in zonal location of the centre in SSTAs and thermocline anomalies are largely due to the different roles of the zonal advective feedback (ZAF) and thermocline feedback (TF). **c**, Growth rates of the two eigenmodes as a function of the mean thermocline depth, *H*, and the mean strength of equatorial trade winds relative to climatological conditions. Black dots mark the mean state for the modes displayed in **a** and **b**. **d**–**f**, Patterns of SSTAs[26] and equatorial Tropical Atmosphere Ocean (TAO)/ Triangle Trans-Ocean Buoy Network (TRITON) 20 °C thermocline depth anomalies for typical EP (1997/1998) and CP (2009/2010) El Niño and La Niña (boreal winter 2010) events (November–January), with schematic representations of the key excitation, nonlinear and cross-scale interaction mechanisms: annual cycle (ACY), WWEs, South Pacific booster (SPB), North and South Pacific meridional modes (NPMM and SPMM, respectively) and tropical instabilty waves (TIW). The solid red, eastward (blue, westward) arrows represent the ZAF and the red, upward (blue, downward) arrows denote the TF for El Niño (La Niña) conditions. The relative sizes and different zonal positions of the arrows indicate qualitatively the strength and areas of strong feedback efficiency. Curly upward (downward) arrows denote damping net surface heat flux (HF) feedback for El Niño (La Niña).

At the heart of our explanation for the spatial flavours of ENSO is the aforementioned multiplicity of coupled ENSO eigenmodes (Fig. 5a, b), as seen in an intermediate ENSO model[46]. Furthermore, the temporal complexity is generated in part by the different oscillation frequencies of the quasi-quadrennial and quasi-biennial modes and additionally by different external excitation processes. Such processes are associated, for example, with the North and South Pacific meridional modes[81,82], the South Pacific booster[38], WWEs (see 'Space–time complexity of ENSO' and 'Seasonal ENSO dynamics'), tropical instability waves[83] or transbasin influences[40] (Fig. 5). In particular, asymmetric dependencies related to the increased WWE activity during El Niño and enhanced tropical instability wave activity during La Niña make these cross-scale interactions very effective sources for ENSO complexity. Furthermore, the annual cycle of winds and SSTs has a key role in determining the seasonal timing of ENSO anomalies and its predictability (see 'Seasonal ENSO dynamics' and 'ENSO predictability'). To further explain the fact that El Niño anomalies are stronger in amplitude (see 'A conceptual view of ENSO dynamics') and exhibit a more pronounced spatial

diversity (see 'Space–time complexity of ENSO') and higher predictability[84] relative to their La Niña counterparts (Figs. 4b, d, 5c, e), we need to invoke additional nonlinear processes. Nonlinearities, particularly in atmospheric deep convection and oceanic heat advection, can induce a wide range of additional timescales[64] and new spatial structures[85,86] by potentially coupling or amplifying the duplet of ENSO eigenmodes.

Decadal subsurface processes[87,88] can affect the long-term climatological background state. In turn, this background state changes the stability of the two primary ENSO eigenmodes (Fig. 5a, b) and their excitability. Hence, slow background state changes in the Pacific Ocean can have a key role in generating and modulating the spatio-temporal complexity of ENSO.

Our unifying framework for ENSO complexity (Fig. 5), which identifies key factors for ENSO complexity (primary ENSO eigenmodes, excitation processes, nonlinearities and cross-timescale interactions), may serve as a roadmap for further hypothesis testing, process studies and diagnostic analysis of climate models. It can also help guide the evolution of the tropical Pacific observing system, which is essential for underpinning ENSO research and forecasting[89]. In addition, this framework can be used to determine how the shortcomings in representing ENSO complexity in climate and Earth system models are related to a variety of feedback processes and biases in the mean state and annual cycle that affect the generation of climate variability.

Outlook

The reliability of dynamical seasonal climate predictions depends heavily on the representation of ENSO processes in CGCMs and on the continuous improvement of the global ocean observing system. Climate models still exhibit stubborn climate biases in the eastern equatorial Pacific[90] that may affect their representation of feedbacks (see 'A conceptual view of ENSO dynamics') and ENSO complexity[47], as well as the fidelity of operational ENSO forecasts. Identifying and resolving underlying systematic model biases will help in developing the next generation of models for seamless climate forecasts and projections.

Future research on ENSO complexity needs to address the role of the seasonal cycle for CP ENSO dynamics, the near-absence of spatial diversity for La Niña[29] (Fig. 5e), the impact of decadal background-state changes on ENSO modes vis-à-vis multiple-timescale processes involving WWEs, tropical instability waves, extratropical triggers, as well as the response of the spatio-temporal complexity of ENSO to past and future climate change. Moreover, whether the underlying dynamical origin of spatio-temporal diversity in CGCMs can in fact be linked to the duplet of quasi-quadrennial and quasi-biennial ENSO eigenmodes must be investigated. This can be tested by applying interactive atmosphere ensemble averaging techniques in coupled climate models[91], which artificially reduce non-SST-related atmospheric perturbations. Moreover, the use of flux-adjusted CGCMs[92] could help elucidate how model biases impact the spatial diversity of ENSO and provide a more effective way of improving seasonal climate predictions. Such experiments could reveal if there are distinct precursors for ENSO diversity, which could be used to further inform ENSO forecasts. Much scientific emphasis has been placed on understanding the growth of El Niño events. However, given the severe impacts of La Niña—for example, on drought in the southwestern United States[93] or the Horn of Africa[94]—and the fact that La Niña events may last longer than one year (Fig. 4), it will be paramount to gain also deeper understanding of the processes controlling La Niña and its predictability through observational, diagnostic and modelling studies.

A growing global population in the 21st century has become increasingly vulnerable to natural hazards as human activities alter the climate and the environment. Society therefore has an urgent demand for better climate products and services, including improved ENSO monitoring and predictions and long-term projections, to better inform decision making for agriculture and food security, public health, water resource management, energy production, human migration and disaster risk reduction. Because ENSO involves a broad range of disciplines, from atmosphere and ocean dynamics, to ecosystems and societal impacts, it is a unifying concept in Earth system science[95]. Thus, our proposed framework for ENSO complexity can serve as both a catalyst to further research and, in its practical applications, an essential contributor for sustainable development and environmental stewardship in a changing world.

Received: 25 October 2017; Accepted: 2 March 2018;
Published online 25 July 2018.

1. Carrillo, C. N. Hidrografía oceánica. *Bol. Soc. Geogr. Lima* **1**, 72–110 (1893).
2. Bjerknes, J. Atmospheric teleconnections from the equatorial Pacific. *Mon. Weath. Rev.* **97**, 163–172 (1969).
3. McPhaden, M. J., Busalacchi, A. J. & Anderson, D. L. T. A TOGA retrospective. *Oceanography* **23**, 86–103 (2010).
4. Cai, W. J. et al. More extreme swings of the South Pacific convergence zone due to greenhouse warming. *Nature* **488**, 365–369 (2012).
5. Capotondi, A. et al. Understanding ENSO diversity. *Bull. Am. Meteorol. Soc.* **96**, 921–938 (2015).
6. Kug, J. S., Jin, F. F. & An, S. I. Two types of El Niño events: cold tongue El Niño and warm pool El Niño. *J. Clim.* **22**, 1499–1515 (2009).
This study demonstrates that the two types of El Niño (CP and EP) have different dynamical structures, including discharge processes and dominant SST feedbacks.
7. Ashok, K., Behera, S. K., Rao, S. A., Weng, H. Y. & Yamagata, T. El Niño Modoki and its possible teleconnection. *J. Geophys. Res. Oceans* **112**, C11007 (2007).
8. Takahashi, K., Montecinos, A., Goubanova, K. & Dewitte, B. ENSO regimes: reinterpreting the canonical and Modoki El Niño. *Geophys. Res. Lett.* **38**, L10704 (2011).
9. Tziperman, E. & Yu, L. S. Quantifying the dependence of westerly wind bursts on the large-scale tropical Pacific SST. *J. Clim.* **20**, 2760–2768 (2007).
10. Lengaigne, M. et al. Triggering of El Niño by westerly wind events in a coupled general circulation model. *Clim. Dyn.* **23**, 601–620 (2004).
11. Choi, J., An, S. I. & Yeh, S. W. Decadal amplitude modulation of two types of ENSO and its relationship with the mean state. *Clim. Dyn.* **38**, 2631–2644 (2012).
12. L'Heureux, M. L. et al. Observing and predicting the 2015/16 El Niño. *Bull. Am. Meteorol. Soc.* **98**, 1363–1382 (2017).
13. Jin, F. F., Kim, S. T. & Bejarano, L. A coupled-stability index for ENSO. *Geophys. Res. Lett.* **33**, L23708 (2006).
14. Hoerling, M. P. & Kumar, A. Why do North American climate anomalies differ from one El Niño event to another? *Geophys. Res. Lett.* **24**, 1059–1062 (1997).
15. Karoly, D. J. & Hoskins, B. J. 3 dimensional propagation of planetary waves. *J. Meteorol. Soc. Jpn* **60**, 109–123 (1982).
16. Ropelewski, C. F. & Halpert, M. S. Global and regional scale precipitation patterns associated with the El-Niño Southern Oscillation. *Mon. Weath. Rev.* **115**, 1606–1626 (1987).
17. Larkin, N. K. & Harrison, D. E. On the definition of El Niño and associated seasonal average US weather anomalies. *Geophys. Res. Lett.* **32**, L13705 (2005).
18. Cobb, K. M. et al. Highly variable El Niño-Southern Oscillation throughout the holocene. *Science* **339**, 67–70 (2013).
19. McGregor, S., Timmermann, A., England, M. H., Timm, O. E. & Wittenberg, A. T. Inferred changes in El Niño–Southern Oscillation variance over the past six centuries. *Clim. Past* **9**, 2269–2284 (2013).
This study uses multi-proxy data to demonstrate that ENSO variance has increased over the past century relative to the previous 500 years.
20. Cai, W. J. et al. ENSO and greenhouse warming. *Nat. Clim. Change* **5**, 849–859 (2015).
21. Rasmusson, E. M. & Carpenter, T. H. Variations in tropical sea-surface temperature and surface wind fields associated with the Southern Oscillation El-Niño. *Mon. Weath. Rev.* **110**, 354–384 (1982).
22. Wang, C. Z. On the ENSO mechanisms. *Adv. Atmos. Sci.* **18**, 674–691 (2001).
23. Jin, F. F. An equatorial ocean recharge paradigm for ENSO. Part I: conceptual model. *J. Atmos. Sci.* **54**, 811–829 (1997).
This paper introduces a heuristic model that explains key features of ENSO dynamics, such as the important role of recharge and discharge processes in ENSO.
24. Roberts, A., Guckenheimer, J., Widiasih, E., Timmermann, A. & Jones, C. Mixed-mode oscillations of El Niño-Southern Oscillation. *J. Atmos. Sci.* **73**, 1755–1766 (2016).
25. Levine, A. F. Z. & Jin, F. F. Noise-induced instability in the ENSO recharge oscillator. *J. Atmos. Sci.* **67**, 529–542 (2010).
26. Rayner, N. A. et al. Global analyses of sea surface temperature, sea ice, and night marine air temperature since the late nineteenth century. *J. Geophys. Res. Atmos.* **108**, 4407 (2003).
27. Giese, B. S. & Ray, S. El Niño variability in simple ocean data assimilation (SODA), 1871–2008. *J. Geophys. Res. Oceans* **116**, (2011).
28. Johnson, N. C. How many ENSO flavors can we distinguish? *J. Clim.* **26**, 4816–4827 (2013).
29. Kug, J. S. & Ham, Y. G. Are there two types of La Niña? *Geophys. Res. Lett.* **38**, L16704 (2011).
30. Kao, H. Y. & Yu, J. Y. Contrasting eastern-Pacific and central-Pacific types of ENSO. *J. Clim.* **22**, 615–632 (2009).
31. Lengaigne, M. & Vecchi, G. A. Contrasting the termination of moderate and extreme El Niño events in coupled general circulation models. *Clim. Dyn.* **35**, 299–313 (2010).

32. An, S.-I., Kug, J.-S., Timmermann, A., Kang, I.-S. & Timm, O. The influence of ENSO on the generation of decadal variability in the North Pacific. *J. Clim.* **20**, 667–680 (2007).
33. Deser, C., Simpson, I. R., McKinnon, K. A. & Phillips, A. S. The Northern Hemisphere extratropical atmospheric circulation response to ENSO: how well do we know it and how do we evaluate models accordingly? *J. Clim.* **30**, 5059–5082 (2017).
34. Fedorov, A. V., Hu, S. N., Lengaigne, M. & Guilyardi, E. The impact of westerly wind bursts and ocean initial state on the development, and diversity of El Niño events. *Clim. Dyn.* **44**, 1381–1401 (2015).
35. Seiki, A. & Takayabu, Y. N. Westerly wind bursts and their relationship with intraseasonal variations and ENSO. Part I: statistics. *Mon. Weath. Rev.* **135**, 3325–3345 (2007).
36. Jin, F. F., Lin, L., Timmermann, A. & Zhao, J. Ensemble-mean dynamics of the ENSO recharge oscillator under state-dependent stochastic forcing. *Geophys. Res. Lett.* **34**, L03807 (2007).
37. Vimont, D. J., Battisti, D. S. & Hirst, A. C. The seasonal footprinting mechanism in the CSIRO general circulation models. *J. Clim.* **16**, 2653–2667 (2003).
This article presents a coupled air-sea mechanism by which extratropical Pacific climate anomalies can propagate into the tropics.
38. Hong, L. C. L Ho & Jin, F. F. A Southern Hemisphere booster of super El Niño. *Geophys. Res. Lett.* **41**, 2142–2149 (2014).
39. Ham, Y. G., Kug, J. S., Park, J. Y. & Jin, F. F. Sea surface temperature in the north tropical Atlantic as a trigger for El Niño/Southern Oscillation events. *Nat. Geosci.* **6**, 112–116 (2013).
40. Chikamoto, Y. et al. Skilful multi-year predictions of tropical trans-basin climate variability. *Nat. Commun.* **6**, 6869 (2015).
This article documents the impact of Atlantic SSTAs on the generation of CP El Niño events.
41. Yu, J. Y. & Kim, S. T. Relationships between extratropical sea level pressure variations and the central Pacific and eastern Pacific types of ENSO. *J. Clim.* **24**, 708–720 (2011).
42. Lee, T. & McPhaden, M. J. Increasing intensity of El Niño in the central-equatorial Pacific. *Geophys. Res. Lett.* **37**, L14603 (2010).
43. Wittenberg, A. T., Rosati, A., Delworth, T. L., Vecchi, G. A. & Zeng, F. R. ENSO modulation: is it decadally predictable? *J. Clim.* **27**, 2667–2681 (2014).
44. Yeh, S. W. et al. El Niño in a changing climate. *Nature* **461**, 511–514 (2009); erratum 462, 674 (2009).
45. Capotondi, A. & Sardeshmukh, P. D. Optimal precursors of different types of ENSO events. *Geophys. Res. Lett.* **42**, 9952–9960 (2015).
46. Xie, R. & Jin, F.-F. Two leading ENSO modes and El Niño Types in the Zebiak–Cane Model. *J. Clim.* (2018).
This study provides theoretical evidence for two coupled modes that resemble EP and CP El Niño events with different timescales and background-state sensitivities.
47. Ham, Y. G. & Kug, J. S. How well do current climate models simulate two types of El Niño? *Clim. Dyn.* **39**, 383–398 (2012).
This work shows that current climate models tend to underestimate the diversity of El Niño owing to dry and cold biases in the equatorial central Pacific.
48. Bellenger, H., Guilyardi, E., Leloup, J., Lengaigne, M. & Vialard, J. ENSO representation in climate models: from CMIP3 to CMIP5. *Clim. Dyn.* **42**, 1999–2018 (2014).
49. Bayr, T. et al. Mean-state dependence of ENSO atmospheric feedbacks in climate models. *Clim. Dyn.* **50**, 3171–3194 (2017).
50. Li, T. Phase transition of the El Niño Southern Oscillation: a stationary SST mode. *J. Atmos. Sci.* **54**, 2872–2887 (1997).
This study applied seasonally varying instability to model coupled ENSO dynamics.
51. Zhang, W. J. et al. Unraveling El Niño's impact on the East Asian monsoon and Yangtze River summer flooding. *Geophys. Res. Lett.* **43**, 11375–11382 (2016).
52. Trenberth, K. E. et al. Progress during TOGA in understanding and modeling global teleconnections associated with tropical sea surface temperatures. *J. Geophys. Res. Oceans* **103**, 14291–14324 (1998).
53. Risbey, J. S., Pook, M. J., McIntosh, P. C., Wheeler, M. C. & Hendon, H. H. On the remote drivers of rainfall variability in Australia. *Mon. Weath. Rev.* **137**, 3233–3253 (2009).
54. McPhaden, M. J. Genesis and evolution of the 1997–98 El Niño. *Science* **283**, 950–954 (1999).
55. Vecchi, G. A. & Harrison, D. E. Tropical Pacific sea surface temperature anomalies, El Niño, and equatorial westerly wind events. *J. Clim.* **13**, 1814–1830 (2000).
56. Wengel, C., Latif, M., Park, W., Harlass, J. & Bayr, T. Seasonal ENSO phase locking in the Kiel Climate Model: the importance of the equatorial cold sea surface temperature bias. *Clim. Dyn.* **50**, 901–919 (2017).
57. Zebiak, S. E. & Cane, M. A. A model El-Niño Southern Oscillation. *Mon. Weath. Rev.* **115**, 2262–2278 (1987).
58. Tziperman, E., Zebiak, S. E. & Cane, M. A. Mechanisms of seasonal–ENSO interaction. *J. Atmos. Sci.* **54**, 61–71 (1997).
59. Galanti, E. et al. The equatorial thermocline outcropping—a seasonal control on the tropical Pacific Ocean–atmosphere instability strength. *J. Clim.* **15**, 2721–2739 (2002).
60. Dommenget, D. & Yu, Y. S. The seasonally changing cloud feedbacks contribution to the ENSO seasonal phase-locking. *Clim. Dyn.* **47**, 3661–3672 (2016).
61. Harrison, D. E. & Vecchi, G. A. On the termination of El Niño. *Geophys. Res. Lett.* **26**, 1593–1596 (1999).
62. Lengaigne, M., Boulanger, J. P., Menkes, C. & Spencer, H. Influence of the seasonal cycle on the termination of El Niño events in a coupled general circulation model. *J. Clim.* **19**, 1850–1868 (2006).
63. McGregor, S., Timmermann, A., Schneider, N., Stuecker, M. F. & England, M. H. The effect of the south Pacific convergence zone on the termination of El Niño events and the meridional asymmetry of ENSO. *J. Clim.* **25**, 5566–5586 (2012).
This work demonstrates that the southward wind shift that leads to the rapid decay of El Niño events is related to the seasonal formation of the South Pacific Convergence Zone.
64. Stuecker, M. F., Timmermann, A., Jin, F. F., McGregor, S. & Ren, H. L. A combination mode of the annual cycle and the El Niño/Southern Oscillation. *Nat. Geosci.* **6**, 540–544 (2013).
65. Stuecker, M. F., Jin, F. F., Timmermann, A. & McGregor, S. Combination mode dynamics of the anomalous northwest Pacific anticyclone. *J. Clim.* **28**, 1093–1111 (2015).
66. Meinen, C. S. & McPhaden, M. J. Observations of warm water volume changes in the equatorial Pacific and their relationship to El Niño and La Niña. *J. Clim.* **13**, 3551–3559 (2000).
67. Barnston, A., Tippett, M. K., Ranganathan, M. & L'Heureux, M. Deterministic skill of ENSO predictions from the North American Multimodel Ensemble. *Clim. Dyn.* https://doi.org/10.1007/s00382-017-3603-3 (2017); erratum https://doi.org/10.1007/s00382-017-3814-7 (2017)
68. Ramesh, N. & Murtugudde, R. All flavours of El Niño have similar early subsurface origins. *Nat. Clim. Change* **3**, 42–46 (2013).
69. Ballester, J., Bordoni, S., Petrova, D. & Rodo, X. Heat advection processes leading to El Niño events as depicted by an ensemble of ocean assimilation products. *J. Geophys. Res. Oceans* **121**, 3710–3729 (2016).
70. Izumo, T. et al. Influence of the state of the Indian Ocean Dipole on the following year's El Niño. *Nat. Geosci.* **3**, 168–172 (2010).
71. Ham, Y. G., Kug, J. S. & Park, J. Y. Two distinct roles of Atlantic SSTs in ENSO variability: North Tropical Atlantic SST and Atlantic Niño. *Geophys. Res. Lett.* **40**, 4012–4017 (2013).
72. Takahashi, K. & Dewitte, B. Strong and moderate nonlinear El Niño regimes. *Clim. Dyn.* **46**, 1627–1645 (2016).
73. Barnston, A. G., Tippett, M. K., L'Heureux, M. L., Li, S. H. & DeWitt, D. G. Skill of real-time seasonal ENSO model predictions during 2002–11: is our capability increasing? *Bull. Am. Meteorol. Soc.* **93**, 631–651 (2012).
74. Newman, M. & Sardeshmukh, P. D. Are we near the predictability limit of tropical Indo-Pacific sea surface temperatures? *Geophys. Res. Lett.* **44**, 8520–8529 (2017).
75. Petrova, D., Koopman, S. J., Ballester, J. & Rodo, X. Improving the long-lead predictability of El Niño using a novel forecasting scheme based on a dynamic components model. *Clim. Dyn.* **48**, 1249–1276 (2017).
76. Kessler, W. S. Is ENSO a cycle or a series of events? *Geophys. Res. Lett.* **29**, 2125 (2002).
This study challenges the notion of ENSO as a cycle and highlights the fact that the ENSO system can lose its dynamical memory during long La Niña events.
77. Barnston, A. G. & Tippett, M. K. Do statistical pattern corrections improve seasonal climate predictions in the North American Multimodel Ensemble models? *J. Clim.* **30**, 8335–8355 (2017).
78. DiNezio, P. N., Deser, C., Okumura, Y. & Karspeck, A. Predictability of 2-year La Niña events in a coupled general circulation model. *Clim. Dyn.* **49**, 4237–4261 (2017).
79. McPhaden, M. J. A. 21st century shift in the relationship between ENSO SST and warm water volume anomalies. *Geophys. Res. Lett.* **39**, L09706 (2012).
80. Jeong, H. I. et al. Assessment of the APCC coupled MME suite in predicting the distinctive climate impacts of two flavors of ENSO during boreal winter. *Clim. Dyn.* **39**, 475–493 (2012).
81. Larson, S. & Kirtman, B. The Pacific Meridional Mode as a trigger for ENSO in a high-resolution coupled model. *Geophys. Res. Lett.* **40**, 3189–3194 (2013).
82. Zhang, H. H., Clement, A. & Di Nezio, P. The south Pacific meridional mode: a mechanism for ENSO-like variability. *J. Clim.* **27**, 769–783 (2014).
83. An, S. I. Interannual variations of the Tropical Ocean instability wave and ENSO. *J. Clim.* **21**, 3680–3686 (2008).
84. Larson, S. M. & Kirtman, B. P. Linking preconditioning to extreme ENSO events and reduced ensemble spread. *Clim. Dyn.* https://doi.org/10.1007/s00382-017-3791-x (2017).
85. Chen, N. & Majda, A. J. Simple dynamical models capturing the key features of the Central Pacific El Niño. *Proc. Natl Acad. Sci. USA* **113**, 11732–11737 (2016).
86. Hao, Z., Neelin, J. D. & Jin, F. F. Nonlinear tropical air-sea interaction in the fast-wave limit. *J. Clim.* **6**, 1523–1544 (1993).
87. Schneider, N. The response of tropical climate to the equatorial emergence of spiciness anomalies. *J. Clim.* **17**, 1083–1095 (2004).
88. McGregor, S., Sen Gupta, A., Holbrook, N. J. & Power, S. B. The modulation of ENSO variability in CCSM3 by extratropical Rossby waves. *J. Clim.* **22**, 5839–5853 (2009).
89. Xue, Y. et al. A real-time ocean reanalyses intercomparison project in the context of tropical pacific observing system and ENSO monitoring. *Clim. Dyn.* **49**, 3647–3672 (2017).
90. Widlansky, M. J. et al. Changes in South Pacific rainfall bands in a warming climate. *Nat. Clim. Change* **3**, 417–423 (2013).
91. Kirtman, B. P., Straus, D. M., Min, D. H., Schneider, E. K. & Siqueira, L. Toward linking weather and climate in the interactive ensemble NCAR climate model. *Geophys. Res. Lett.* **36**, (2009).

92. Vecchi, G. A. et al. On the seasonal forecasting of regional tropical cyclone activity. *J. Clim.* **27**, 7994–8016 (2014).
93. Cook, E. R., Seager, R., Cane, M. A. & Stahle, D. W. North American drought: reconstructions, causes, and consequences. *Earth Sci. Rev.* **81**, 93–134 (2007).
94. Nicholson, S. E. & Selato, J. C. The influence of La Niña on African rainfall. *Int. J. Climatol.* **20**, 1761–1776 (2000).
95. McPhaden, M. J., Zebiak, S. E. & Glantz, M. H. ENSO as an integrating concept in Earth science. *Science* **314**, 1740–1745 (2006).
96. Balmaseda, M. A., Mogensen, K. & Weaver, A. T. Evaluation of the ECMWF ocean reanalysis system ORAS4. *Q. J. R. Meteorol. Soc.* **139**, 1132–1161 (2013).
97. Huang, B. Y. et al. Extended reconstructed sea surface temperature, version 5 (ERSSTv5): upgrades, validations, and intercomparisons. *J. Clim.* **30**, 8179–8205 (2017).
98. Penny, S. G., Behringer, D. W., Carton, J. A. & Kalnay, E. A hybrid global ocean data assimilation system at NCEP. *Mon. Weath. Rev.* **143**, 4660–4677 (2015).
99. Puy, M., Vialard, J., Lengaigne, M. & Guilyardi, E. Modulation of equatorial Pacific westerly/easterly wind events by the Madden–Julian oscillation and convectively-coupled Rossby waves. *Clim. Dyn.* **46**, 2155–2178 (2016).
100. Adler, R. F. et al. The version-2 global precipitation climatology project (GPCP) monthly precipitation analysis (1979–present). *J. Hydrometeorol.* **4**, 1147–1167 (2003).

Acknowledgements A.T., K.S., K.-S.Y. and E.Z. were supported by the Institute for Basic Science (project code IBS-R028-D1). B.D. was funded by Fondecyt (grant 1151185). S.-I.A. was supported by the Basic Science Research Program through the National Research Foundation of Korea (NRF-2017R1A2A2A05069383). J.-S.K. was supported by the National Research Foundation of Korea (NRF-2017R1A2B3011511). F.-F.J.'s contribution was sponsored through the US NSF Grant AGS-1406601 and the US Department of Energy Grant DE-SC0005110. T.B. receives funding from SFB 754, project 'Climate–Biochemistry Interactions in the tropical Ocean'. M.J.M. is supported by the US National Oceanic and Atmospheric Administration (NOAA). H.-L.R. is supported by the China Meteorological Special Research Project (grant number GYHY201506013). S.I. was supported by the UK–China Research & Innovation Partnership Fund through the Met Office Climate Science for Service Partnership (CSSP) China as part of the Newton Fund. M.F.S. acknowledges support from the NOAA Climate and Global Change Postdoctoral Fellowship Program, administered by UCAR's Cooperative Programs for the Advancement of Earth System Sciences (CPAESS). H.R. was partly funded by the National Environmental Science Program, Australia. This is PMEL contribution number 4723. The authors thank the TAO Project Office of NOAA/PMEL for providing the TAO/TRITON 20 °C isotherm depth anomaly data shown in Fig. 5.

Reviewer information *Nature* thanks M. L'Heureux, X. Rodo and A. Tudhope for their contribution to the peer review of this work.

Author contributions The manuscript was written as a group effort during the 'El Niño Complexity workshop', held at Pusan National University from 16 to 20 October 2017. All authors contributed to the manuscript preparation and the discussions that led to the final figure selection. A.T., J.-S.K., S.-I.A. and F.-F.J. designed the study and served as coordinating lead authors for the sections 'ENSO predictability', 'Space–time complexity of ENSO', 'A conceptual view of ENSO dynamics' and 'A unifying framework', respectively. A.T. oversaw the writing of each section, preparation of figures and selection of references. W.C., A.C. K.M.C., M.L., M.J.M, M.F.S and A.T.W. served as coordinating lead authors for various sections.

Competing interests The authors declare no competing interests.

Additional information
Reprints and permissions information is available at http://www.nature.com/reprints.
Correspondence and requests for materials should be addressed to A.T.
Publisher's note: Springer Nature remains neutral with regard to jurisdictional claims in published maps and institutional affiliations.